J. Adv. Oxid. Technol. V.6, N1, 23-29, (2003)

KINETICS, PRODUCTS AND MECHANISM OF DESTRUCTION OF ETHANE IN CORONA DISCHARGE

Anatoli A. Chernov,[1] Larisa G. Krishtopa,[1] Oleg P. Korobeinichev,[2] and Lev N. Krasnoperov[*1]

[1]*Department of Chemistry and Environmental Science, New Jersey Institute of Technology, Newark, NJ 07102, U. S. A.*

[2]*Institute of Chemical Kinetics and Combustion, Siberian Branch of Russian Academy of Sciences, Novosibirsk, 630090, Russia*

*Author to whom correspondence should be sent:

Professor Lev Krasnoperov
Department of Chemistry and Environmental Science
New Jersey Institute of Technology
University Heights
Newark, NJ 07102

E-mail: krasnoperov@adm.njit.edu

Abstract

Destruction of ethane in corona discharge was studied using a tubular coaxial wire AC high-voltage dielectric barrier discharge flow reactor coupled to a GC/MS and a quadrupole mass-spectrometer. The experiments were performed at ambient temperature (298 ± 3 K) and pressure (1.00 ± 0.04 bar). Mixtures of 12, 109, 1033 and 10000 ppm ethane in synthetic air (21% O_2, 79% N_2) were passed through the reactor with the flow rates in the range 0.17 - 4.8 sccs. The active discharge power was varied in the range 0.01 - 4.0 W. The reactant (ethane) and the products of the destruction were monitored on line using the electron impact MS as well as the GC/MS. The degree of the destruction was measured at different ethane concentrations, flow rates, and the discharge powers. The measured dependences of ethane concentration on the specific absorbed energy are double-exponential. The energy efficiencies and the G-values were determined. In addition to H_2O, CO_2 and CO, acetic acid (CH_3COOH), ethyl nitrate ($C_2H_5ONO_2$), methyl nitrate (CH_3ONO_2), ethanol (C_2H_5OH), and nitromethane (CH_3NO_2) were identified among the major destruction products. The experimental results are in discrepancy with a detailed free-radical reaction based model. The discrepancy in the destruction energy efficiency increases at low concentrations of ethane and reaches a factor of 10000 at 12 ppm.

Introduction

During the last decade, corona discharge received significant attention as a prospective technology for cleaning contaminated air flows (1 - 21). The approach appeared to be almost universal and was considered for hydrocarbons ("VOCs") (1 - 6), organophosphorous compounds (7 - 9), NO_x (10 - 14), SO_x (14 - 17), soot (18) and fluorohalocarbons (freons) (19) destruction. Although a large number of applied investigations were performed (2 - 20), the mechanism of the destruction was not established with certainty. At the early stages the "free-radical" mechanism for hydrocarbon destruction was generally assumed (20). However, even then, the basic difficulties of the free-radical mechanism were apparent (1). Simple estimates (as well as the detailed mechanistic calculations for methane) were in quantitative discrepancy with the experimental data up to three orders of magnitude (1). However, with respect to the kinetics and the efficiency of the destruction in corona discharge methane is not a true representative but rather an exception in the hydrocarbon family (1).

The current work is a detailed experimental study of the destruction of ethane in corona discharge. It was predicted (and confirmed in the current experiments) that ethane will exhibit a similar behavior as the majority of hydrocarbons with respect to the destruction in corona discharge. Such a prediction was made based on the ionization energy of ethane in comparison with the ionization energies of molecular oxygen – the correlation outlined earlier based on the extensive study of the destruction of a number of hydrocarbons and other molecules in corona discharge (1). Ethane is the simplest hydrocarbon molecule after methane. Therefore, a reliable elementary reaction model for ethane oxidation can be built and compared with the experimental results.

Experimental

A tubular dielectric barrier AC corona discharge reactor coupled to a mass-spectrometer and a GC/MS (Fig. 1) was used to study the efficiency and the kinetics of C_2H_6 destruction in air at concentrations in the range 12 - 10000 ppm. The flow reactors used were Pyrex glass tubes (length 80 cm, I.D. = 4 mm) with a thin Ni-Cr coaxial wire (0.43 mm in diameter) used as a high-voltage electrode. The second (grounded) electrode is made from aluminum foil wrapped outside the tube. Corona discharge was excited by application of high AC voltage (up to 20 kV, 60 Hz) to the central wire. This arrangement results in a uniform discharge along the length of the reactor. The reactant (C_2H_6) and the products of the destruction were monitored on-line by a quadruple mass spectrometer Finnigan 4021 and by a 5973 HP GC/MS equipped with a Valco 6-port valve with a 0.25 ml sampling loop. The efficiency of the destruction was studied as a function of the active power dissipated in the reactor, the reactor residence time, the flow rate and the concentration of ethane. The reactor temperature was sustained at 22 ± 2 ^{o}C.

... Figure 1 goes near here ...

Determinations of the active power absorbed in the reactor were based on the current-voltage measurements. The output voltage of the high voltage transformer was measured using a two-resistor voltage divider. The discharge current was monitored by measuring the voltage across a resistor connected in series with the output grounded wire. Oscilloscope traces of the voltage and current recorded using a digital oscilloscope (HP 54501) were multiplied and averaged to produce the average value of the active power. The parasitic losses in the high-voltage transformer were determined in the same manner with reactor disconnected from the high-

voltage cable. These losses were subtracted from the active power measured with the reactor connected to the high-voltage power supply. The discharge power was varied by varying the input voltage of the high-voltage transformer over the range 0 – 8 W.

The ion source temperature of the quadrupole MS was kept at 40 ^{o}C. In the current work, due to the interference of the background mass-spectrum, no attempt to quantify the major final products of the destruction (CO, CO_2 and H_2O), was made. The research was mainly focused on the other carbon and nitrogen containing products of the destruction.

Chromatographic separations and analyses were performed using two capillary columns: 30 m x 0.25 mm HP-5MS column and 50 m x 0.25 mm Chrompack Al_2O_3/KCl PLOT column.

Calibration of the GC/MS was performed using gas calibration mixtures prepared in a 2 L static dilution bottle (Kontess company) with Mininert valve using air as a dilution gas. Mixtures were prepared by injection of measured amounts of liquid compounds by a syringe through the valve into a calibrated volume with subsequent vaporization. Nitromethane, acetaldehyde, propionaldehyde, acetic acid, formic acid, and ethanol, purchased from Aldrich, were used for preparation of the calibration mixtures of these compounds. Ethyl nitrate and methyl nitrate were synthesized (25, 26) and purified before the preparation of the calibration mixtures. All the sensitivity coefficients were determined relative to propanal, used as a standard.

Chrompack Al_2O_3/KCl PLOT column was used to measure concentrations of C_2H_6 and N_2O. This column also ensures analysis of all C_1-C_5 hydrocarbons. However, CH_4, C_2H_4, CH_3OH, and CH_2O, indicated as possible intermediate products of ethane destruction in the preliminary model calculations, were not detected in the experiments. Commercially available gas mixtures of ethane in zero air, 1034 ppm of nitrous oxide (N_2O) in nitrogen (Matheson Tri-Gas, Inc.) and a

multicomponent mixture of 1.00% CO, 1.00% CO_2, 1.00% H_2, 1.01%CH_4, and 1.01% O_2 in nitrogen (Scott Specialty Gases) were also used for the GC/MS calibration.

Two methods were used to protect GS columns from ozone formed in the discharge. The reactor outlet flow was either passed through an additional reactor heated up to 230 ^oC to thermally decompose ozone or through a manganese oxide (Aldrich, catalog #24,344-2) trap at ambient temperature. Manganese oxide is an efficient catalyst of ozone decomposition even at room temperature (27). Destruction of ozone in the samples of the reaction mixture exiting the reactor can potentially affect the mixture composition. Only minor effect of the passing of the outlet mixture through the additional heated reactor or through the manganese oxide trap on the products concentrations was found. Experimentally, it was found that the impact of the ozone destruction in the heated reactor or manganese oxide trap on the concentrations of ethane is less than 10 %. The measurements of the degree of destruction of ethane were performed without using these ozone-destroying devices using the Chrompack Al_2O_3/KCl column, which is relative stable towards ozone.

The concentration of ozone in the output flow from the reactor was measured simultaneously by two independent methods: by UV absorption and by a quadrupole MS. The UV absorption allowed reliable determination of the absolute concentrations of ozone using absorption at the wavelength of 253.7 nm with a 1.00 cm cell. The ozone absorption cross sections at this wavelength is 1.15×10^{-17} cm^2 (28). A small fraction of the flow exiting the cell was sampled into the ion source of the quadrupole MS. The calibration of the MS for ozone was performed by comparison of the MS peak m/z = 48 with the UV absorption. It was found that at temperatures of the ion source above 140 ^oC the MS measurements underdetermined ozone compared to the UV measurements due to the thermal decomposition of ozone in the ion source. Therefore, the

ion source temperature was kept at 40 ^{o}C in the measurements of ozone concentration. In all other experiments the temperature of the ion source was kept at 140 ^{o}C.

... Figure 2 goes near here ...

Results and Discussion

The dependence of the mole fraction of ozone on the specific energy deposition at different concentrations of ethane at the flow rate of 1.2 sccs is shown in Fig. 2. There is only a minor impact of ethane on the ozone production at the concentration of ethane 109 ppm. When 1033 ppm of ethane is used, the outlet ozone concentration is reduced by ca. 30%. Addition of 1% of ethane reduces concentration of ozone 2.6 times.

... Figure 3 goes near here ...

Fig. 3 shows the destruction of 12 ppm ethane in corona discharge as a function of the specific energy deposition at different flow rates. Variation of the flow rate by a factor of four has no impact on the destruction efficiency at a given specific energy deposition, the specific energy deposition being the only parameter that determines the efficiency of the destruction. The dependence of the outlet concentration on the specific absorbed energy has distinct “double-exponential” character.

A similar dependence for 1% C_2H_6 in air is shown in Fig. 4. At this high concentration the dependence is single-exponential. Due to the non-exponential character of the destruction curves

the value of the destruction parameter $E_{v,0}$ (1) defined by equation E1 depends on the specific energy:

$$E_{v,0} = -E_v \ln((C_2H_6)_{out}/(C_2H_6)_{in}) \quad \text{(E1)}$$

In this equation, $(C_2H_6)_{out}$ and $(C_2H_6)_{in}$ are the outlet and the inlet concentrations of ethane, respectively, E_v is the specific deposited energy:

$$E_v = \text{Absorbed Energy / Gas Volume} = \text{Active Power / Volumetric Flow Rate} \quad \text{(E2)}$$

... Figure 4 goes near here ...

The destruction parameters $E_{v,0}$ (defined by equation E1) determined from the experimental data at different concentrations of ethane are shown in Fig. 5. Filled squares refer to a small specific energy of 0.004 J/cm^3 which is equivalent to the definition of $E_{v,0}$ through the initial slopes of the destruction curves (1). In the figure, the destruction parameter determined from the initial slopes (at a small energy deposition of 0.004 J/cm^3) as well as these determined at the specific deposited energy of 1 J/cm^3 are shown vs. the ethane concentration. The efficiency of the destruction in terms of the energy required per unit volume of the gas mixture decreases with ethane concentration. For example, at the lowest concentration used, 12 ppm, the destruction parameter determined using the initial slopes of the destruction curves is 0.067 J/cm^3. The energy consumption increases with the concentration and reaches 8.5 J/cm^3 for 1 % ethane in air.

... Figure 5 goes near here ...

The experimental data were compared with the preliminary calculations using a detailed model of free radical reactions. The model consists of several processes of molecular dissociation by electron impact with subsequent 803 reactions of 87 atoms, free radicals and excited states. The original mechanism of the high-temperature oxidation of hydrocarbons (29), that contains more than 1207 elementary reactions, including reactions of nitrogen-containing species, was modified. Only reactions of C_1 and C_2 species were left in the mechanism (excluding C_2H_5CHO and C_2H_5CO). Reactions involving HOCN, HNCO, C_2N_2, CNN, HCNN, HCNH, N_2H_2, N_2H_3, N_2H_4 were excluded. Additional 79 reactions, important at low temperatures of the current study were added to the mechanism based on the data available in the NIST database (30). Additional 4 reactions of C_2H_5O and CH_3O radical with NO and NO_2 (25, 26) were added to the mechanism.

Initiation of the reaction was described by the formation of oxygen and nitrogen atoms in the ground and the excited electronic states by electron impact dissociation of the major components of the reacting mixture. The initiation processes include electron impact dissociation of molecular oxygen, nitrogen, ozone and water. The rates of formation of ozone measured without ethane added at variable flow rates and the discharge power, were used to calibrate the rates of the initiation reactions forming oxygen atoms.

Preliminary calculations with this detailed mechanism can be summarized as follows. The model qualitatively predicts some of the destruction products. The model predicts the energy efficiency of the destruction factor of 10 *lower* than the experimentally observed for the concentration of ethane of 1%. The discrepancy in the destruction efficiency increases at low

concentrations and reaches a factor of 10^4 at 12 ppm - the experimentally observed destruction efficiency is ca. 10000 times *higher* than the model prediction.

... Figure 6 goes near here ...

Water and carbon dioxide, the final products of the destruction, were observed using the MS detection. Due to the background contributions, no attempt of quantitative measurements of these products was made in this study. A search for CH_4, C_2H_4, CH_2O, and CH_3OH was performed. These products were not detected. The following intermediate products were identified and quantified: acetic acid, ethyl nitrate, methyl nitrate, ethanol and nitromethane.

The relative yields of the products per one ethane molecule destroyed for the 1% and 1033 ppm mixtures of ethane in air are shown in Fig. 6 and 7.

... Figure 7 goes near here ...

The pattern of N-containing products is consistent with the following simplified mechanism. The major C-containing products of the primary steps involving ethane (irrespective of the nature of these processes) are ethyl and methyl radicals, C_2H_5 and CH_3. They can be formed by H-atom abstraction in the free radical reactions, in the ion-molecule reactions, in the reactions of ion-electron dissociative neutralization, and via the direct electron impact dissociation.

It should be noted, that the current model, which does not take into account the ion-molecule reactions, completely fails to explain the absolute energy efficiency of ethane destruction. Still, the spectrum of the products to a significant degree could be determined by the secondary free

radical reactions. Some of the destruction products observed in the current study could be explained by the following elementary reactions.

At not very high temperatures and in the oxygen-containing mixtures peroxy radicals play an important role. As a result, methoxy and ethoxy free radicals are formed (30):

$C_2H_5 + O_2(+M) \longrightarrow C_2H_5O_2(+M)$ (1)

$CH_3 + O_2(+M) \longrightarrow CH_3O_2(+M)$ (2)

$CH_3 + O_3 \longrightarrow CH_3O + O_2$ (3)

$C_2H_5 + O_3 \longrightarrow C_2H_5O + O_2$ (4)

$CH_3O_2 + O \longrightarrow CH_3O + O_2$ (5)

$C_2H_5O_2 + NO_3 \longrightarrow C_2H_5O + NO_2 + O_2$ (6)

$C_2H_5O_2 + NO \longrightarrow C_2H_5O+NO_2$ (7)

$C_2H_5O_2 + C_2H_5O_2 \longrightarrow C_2H_5O+C_2H_5O+O_2$ (8)

$CH_3O_2 + CH_3O_2 \longrightarrow CH_3O+CH_3O+O_2$ (9)

$CH_3O_2+NO \longrightarrow CH_3O+NO_2$ (10)

Further reactions of methoxy, ethoxy, and methyl and ethyl peroxy radicals lead to formation of the observed nitrates (25, 26, 30):

$C_2H_5O + NO_2 \longrightarrow C_2H_5ONO_2$ (11)

$CH_3O + NO_2 \longrightarrow CH_3ONO_2$ (12)

$C_2H_5O_2 + NO \longrightarrow C_2H_5ONO_2$ (13)

$CH_3O_2 + NO \longrightarrow CH_3ONO_2$ (14)

In addition, these products can be formed directly from ethyl and methyl radicals in reactions with NO_3 (30):

$$C_2H_5 + NO_3 \longrightarrow C_2H_5ONO_2 \quad (15)$$

$$CH_3 + NO_3 \longrightarrow CH_3ONO_2 \quad (16)$$

Other observed reaction products, CH_3NO, C_2H_5OH and $CH_3C(O)OH$, are also predicted by the free radical mechanism. Several products, predicted by the model (C_2H_4, CH_4, CH_3OH, and CH_2O), were not observed.

In addition to the observed products, which could be explained by the secondary free radical chemistry, a new compound that reveals itself as a relatively broad peak in the GC - MS chromatograms, was observed. The mass spectrum identification based on the NIST mass spectra library indicated 1,2-propanediol, 3,3”-oxidi,- tetranitrate ($C_6H_{10}N_4O_{13}$), as the product responsible for this peak. Fig. 8 shows the measured dependence of the fraction of the $C_6H_{10}N_4O_{13}$ peak area of the total peak area of all observed products vs. ethane concentration in air for the specific deposited energy of 7.92 J/cm^3 and the gas flow rate of 1.2 cm^3/s. This product represents a relatively minor component at high concentrations of ethane. For example, for 1 % of ethane in air, the peak area of this product is only 3% of the total area of all peaks. The relative abundance of this product increases at low concentrations. At 12 ppm this was the only product of the destruction detected in the experiments (Fig. 8).

... Figure 8 goes near here ...

Currently, the mechanism of formation of this molecule is not clear. A free radical mechanism as well as ion-assisted polymerization could be speculated.

Conclusions

A detailed experimental study of the destruction of ethane in zero air in dielectric barrier corona discharge was performed. The intermediate and minor final products of the destruction were identified and quantified. The energy efficiency of the destruction was determined over a wide range of ethane concentrations (12 - 10000 ppm). The efficiency of the destruction increases at low ethane concentrations in line with the expectations for molecules having ionization energy lower than the energy of ionization of molecular oxygen (1). The free radical model predicts the efficiency almost independent of ethane concentration. The detailed free-radical reaction based model qualitatively predicts some of the destruction products. The experimentally observed energy efficiencies are higher than these predicted by the model. The discrepancy is a factor of 10 for the concentration of ethane of 1%. The discrepancy between the experimentally determined destruction efficiency and predicted by the model increases at low concentrations and reaches a factor of 10^4 at 12 ppm.

A number of the destruction products can be qualitatively explained by the free radical secondary chemistry, while no quantitative agreement can be reached. A new product, tentatively identified as 1,2-propanediol, 3,3”-oxidi-, tetranitrate ($C_6H_{10}N_4O_{13}$), was observed. The relative yield of this product increases at low ethane concentrations. The results of the current study are in agreement with the kinetic characteristics of the destruction of other hydrocarbons in corona discharge.

Acknowledgement

This research was supported by a NATO Linkage Grant DISRM.LG961353 and by a grant from the US Army Research Office DAAG55-98-0068.

References and Notes

1. Krasnoperov, L.N., Krischtopa, L.G., and Bozzelli, J.W., *Journal of Advanced Oxidation Technologies*, **1997**, v.1, No.3, p.97
2. Yamamoto, T.; Ramanathan, K.; Lawless, Ph.A.; Ensor, D.S.; Newsome, J.R.; Plaks, N.; Ramsey, G.H. *IEEE Transactions on Industry Applications*, **1992**, *28*, 3, 528.
3. Storch, D.G.; Kushner, M.J. *J. Appl. Phys.*, **1993**, *73*, 1, 51.
4. Chang, M.B.; Lee, C.C. *Environ. Sci. Technol.*, **1995**, *29*, 181.
5. Sano, N.Z; Nagamoto, T.; Tamon, H.; Suzuki, T.; Okazaki, M. *Ind. Eng. Chem. Res.*, **1997**, *36*, 3783.
6. Fitzimmons, C.; Ismail, F.; Whitehead, J.C.; Wilman, J.J. *J. Phys. Chem.* A, **2000**, *104*, 6032.
7. Clothiaux, E.J.; Koropchak, J.A.; Moore, R.R. *Plasma Chem. Plasma Process.* **1984**, *4*, 15.
8. Fraser, M.E.; Eaton, H.J.; Sheinson, R.S. *Environ. Sci. Technol*, **1985**, *19*, 946.
9. Korobeinichev, O.P.; Chernov, A.A.; Sokolov, V.V.; Krasnoperov, L.N. *Int. Journal of Chemical Kinetics*, **2002**, *34*, 5, 331.
10. Ohkubo, T.; Kanazavwa, S.; Nomoto, Y.; Chang, J.-Sh.; Adachi, T. *IEEE Transactions on Industry Application*, **1994**, *30*, 4, 856.
11. Chang, M.B.; Kushner, M.J.; Rood, M.J. *Environ. Sci., Technol.*, **1992**, *26*, 777.
12. Penetrane, M.B.; Hsiao, M.C.; Merrit, B.T.; Vogtlin, G.E. *IEEE Transaction on Plasma Science*, **1995**, *23*, 4, 679.
13. Urashima, K.; Chang, J.Sh.; Ito, T. *IEEE Transactions on Industry Application*, **1997**, *33*, 4, 879.

14. Masuda, S. *J. Appl. Chem.*, **1988**, *60*, 5, 727.

15. Sun, W.; Pashaie, B.; Dhali, S.K.; Honea, F.I. *J. Appl. Phys.*, **1996**, *79*, 7, 3438.

16. Onda, K.; Kasuga, Y.; Kato, K.; Fujiwara, M.; Tanimoto M. *Energy Convers. Mgmt*, **1997**, *38*, 1377.

17. Chang, M.B.; Balbach, J.H.; Rood, M.J.; Kushner, M.J. *J. Appl. Phys.*, **1991**, *69*, 8, 4409.

18. Harano, A.; Sadakata, M.; Sato, M. *J. Chem. Engin. of Japan*, **1991**, *24*, 1, 100.

19. Spiess, F.J.; Chen, H.; Brock S.L.; Suib, S.L.; Hayashi, Y.; Matsumoto, H. *J. Appl. Phys. A*, **2000**, *104*, 11111.

20. Evans, D.; Rosocha, L.A.; Anderson, G.K.; Coogan, J.J.; Kushner, M.J. *J. Appl. Phys.*, **1993**, *74*, 9, 5378.

21. Urashima, K.; Chang, J.-S. *IEEE Transactions on Industry Application*, **2000**, *7*, 5, 602-613.

22. Eliasson H.M. and Kogelshatz U., *J.Phys.B: Appl. Phys*., **1986**, 22, p.1241

23. Peyrous R., Pignolet P., Held B., *J.Phys.D: Appl. Phys.* **1989**, 22, pp. 1658-1667

24. Berbie M.Penetrane et al *Jpn. J. Appl. Phys.*, **1997**, Vol. 36, Pt.1, No 7B, pp.5007-5017,

25. Ranschaert, D.L., Schneider, N.J., and Elrod M.J., *J. Phys. Chem. A*, **2000**, 104, 5758-5765.

26. Scholtens, K.W., Messerer, B.M., Cappa,C.D., and Elrod M.J., *J. Phys. Chem. A*, **1999**, 103, 4378-4384.

27. Li, W.; Gibbs, G.V.; Oyama, S.T. *J. Phys. Chem. A*, **1998**, *120*, 9041.

28. DeMore, W.B.; Sander, S.p.; Golden, D.M.; Hampson, R.F.; Kurylo, M.J.; Howard, C.J.; Ravishankara, A.R.; Kolb, C.E.; Molina, M.J. *Chemical Kinetics and photochemical Data for use in Stratospheric Modeling.* Evaluation Number 10, **1992**, 106.

29. Konnov, A.A. *Development and validation of a detailed reaction mechanism for the combustion of small hydrocarbons. 28-th Symposium (Int.) on Combustion. Abstr. Symp., Edinburgh*, **2000**, 317.

30. Mallard, W.G.; Westley, F.; Herron,J.T.; Hampson, R.F.; Frizzell, D. NIST Chemical *Kinetics Database - NIST Standard Reference Database 17 - 2Q98.* NIST, Gaithersburg, MD, **1998**.

Figure Captions

Figure 1. Experimental set-up.

Figure 2. Ozone yield vs. the specific energy deposition for different concentrations of ethane in zero air. Open circles - air only (measured using UV absorption). Filled circles - air only (measured using quadrupole MS). Filled squares - 109 ppm (quadrupole MS). Filled triangles down - 1033 ppm (quadrupole MS). Filled triangles up - 1% ethane (quadrupole MS).

Figure 3. Destruction of 12 ppm C_2H_6 in air in corona discharge. Outlet concentration of ethane vs. the specific energy deposition at different gas flow rates. Filled triangles -1.2, open squares - 2.4, filled stars - 4.8 cm^3/sec. The solid line is a double-exponential fit: $[C_2H_6]_{out}/[C_2H_6]_{in} = A*\exp(-E_v/E_{vo,1})+(1-A)*\exp(-E_v/E_{vo,2})$.

Figure 4. Destruction of 1% ppm C_2H_6 in corona discharge. Open squares - 1.2, filled squares - 2.5 cm^3/sec.

Figure 5. Destruction parameter $E_{v,0}$ vs. ethane concentration.

Figure 6. Products yields for $C_2H_5ONO_2$, CH_3ONO_2, CH_3NO, C_2H_5OH, $CH_3C(O)OH$ vs. the specific deposited energy. Destruction of 1% C_2H_6 in air. Gas flow rate 1.2 cm^3/sec.

Figure 7. Products yields for $C_2H_5ONO_2$, CH_3ONO_2, CH_3NO, $CH_3C(O)OH$ vs. the specific deposited energy. Destruction of 1033 ppm C_2H_6 in air. Gas flow rate 1.2 cm^3/sec.

Figure 8. Relative yield of a product identified as $C_6H_{10}N_4O_{13}$ vs. C_2H_6 concentration. Gas flow rate 1.2 cm^3/sec, specific deposited energy 7.92 J/cm^3.

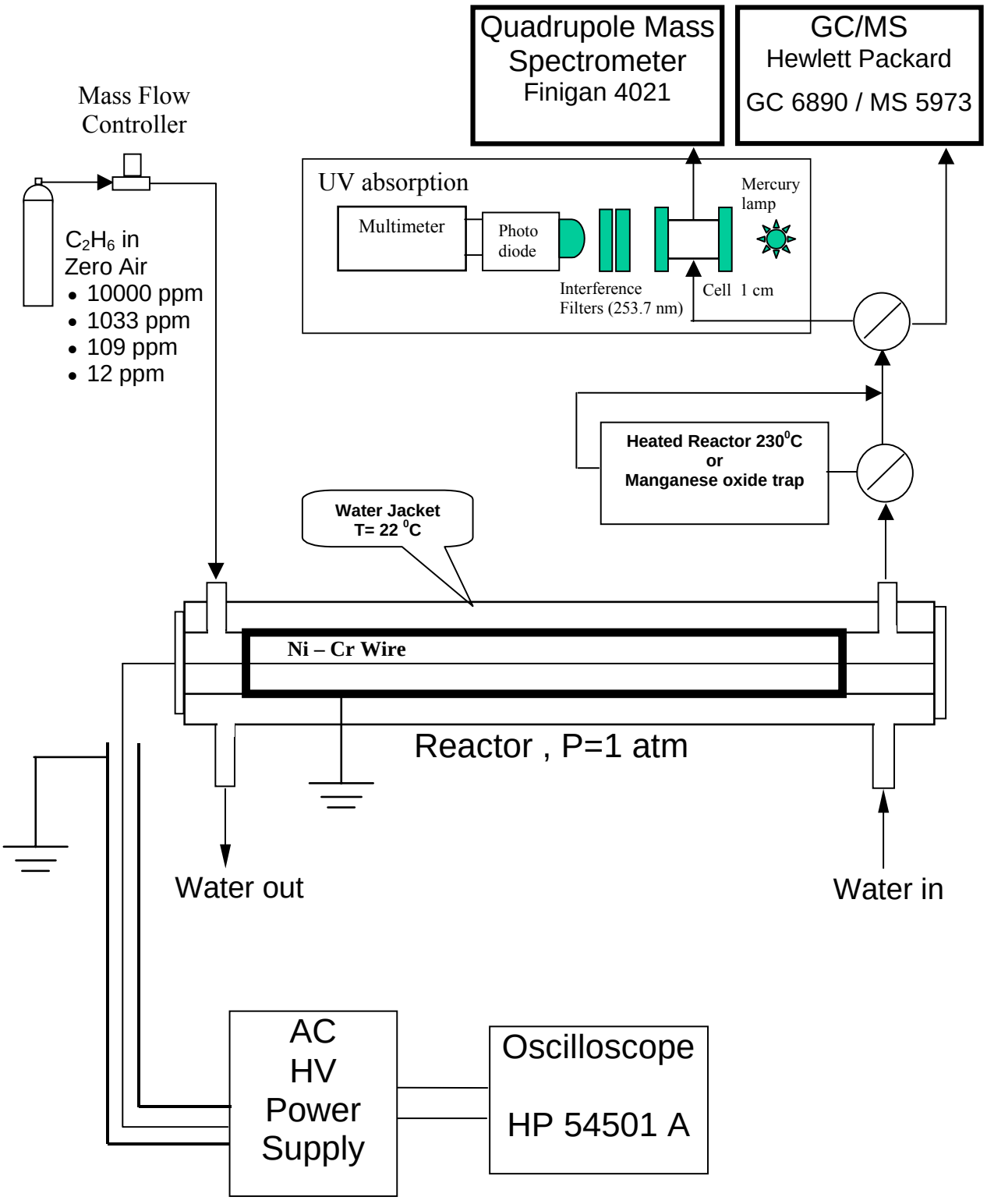
Quadrupole Mass Spectrometer
Finigan 4021
GC/MS
Hewlett Packard
GC 6890 / MS 5973
Mass Flow Controller
UV absorption
Multimeter
Photo diode
Mercury lamp
Interference Filters (253.7 nm)
Cell 1 cm
C2H6 in Zero Air
• 10000 ppm
• 1033 ppm
• 109 ppm
• 12 ppm
Heated Reactor 230°C
or
Manganese oxide trap
Water Jacket
T= 22 °C
Ni – Cr Wire
Reactor , P=1 atm
Water out
Water in
AC HV Power Supply
Oscilloscope
HP 54501 A

Figure 1

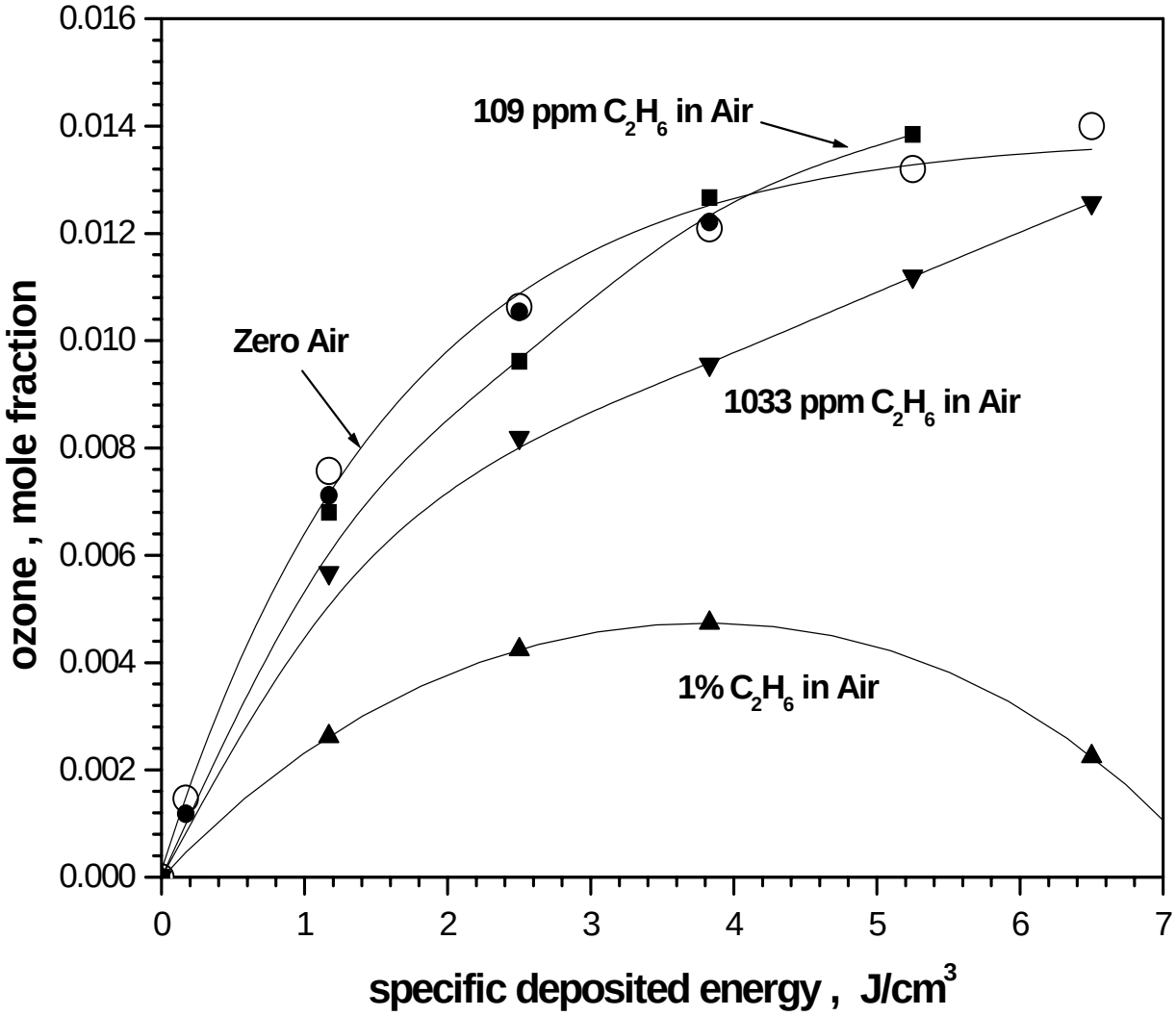
0.016
0.014
0.012
0.010
0.008
0.006
0.004
0.002
0.000
ozone , mole fraction
0
1
2
3
4
5
6
7
specific deposited energy , J/cm3
109 ppm C2H6 in Air
Zero Air
1033 ppm C2H6 in Air
1% C2H6 in Air

Figure 2

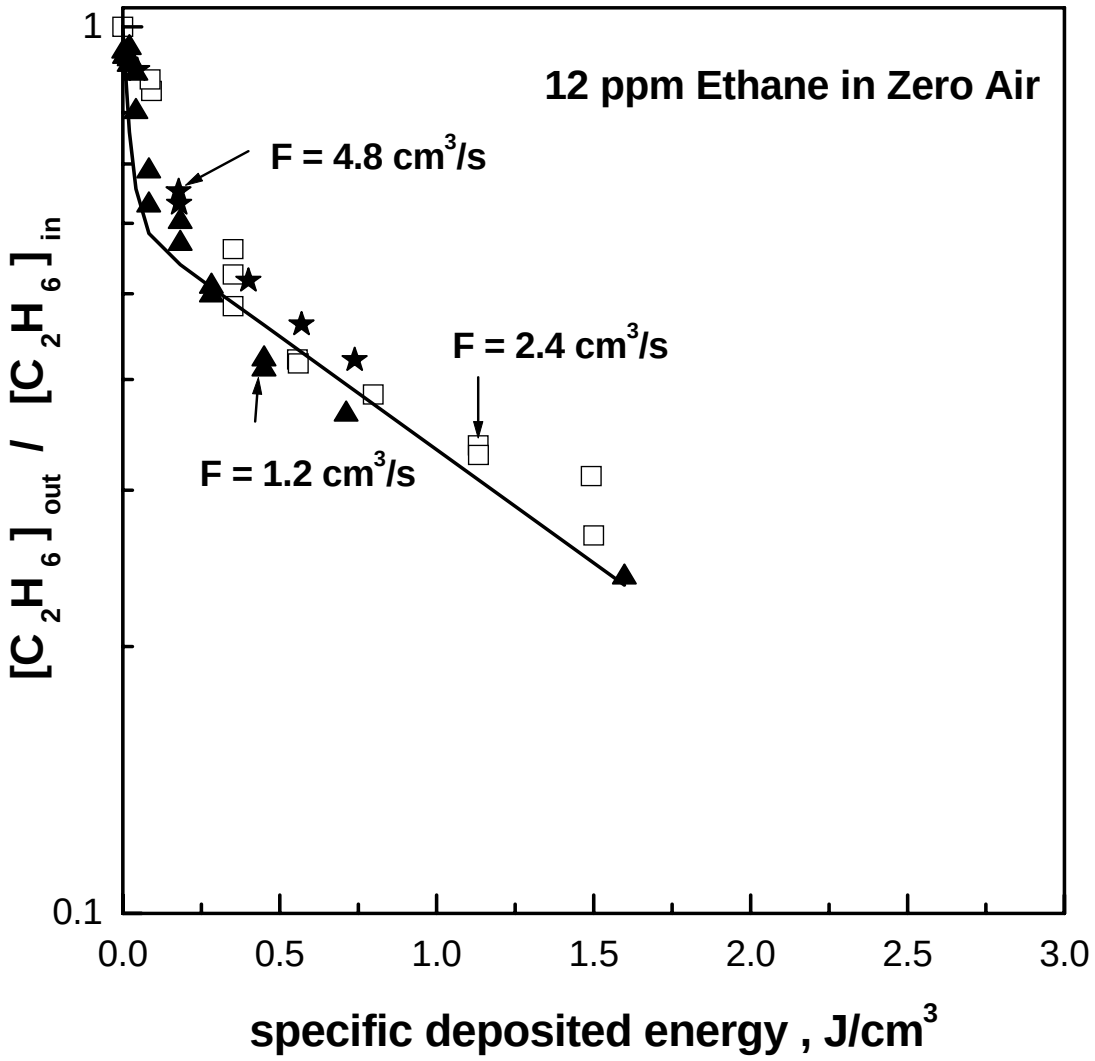
12 ppm Ethane in Zero Air
F = 4.8 cm3/s
F = 2.4 cm3/s
F = 1.2 cm3/s
[C2H6]out / [C2H6]in
specific deposited energy , J/cm3
1
0.1
0.0
0.5
1.0
1.5
2.0
2.5
3.0

Figure 3

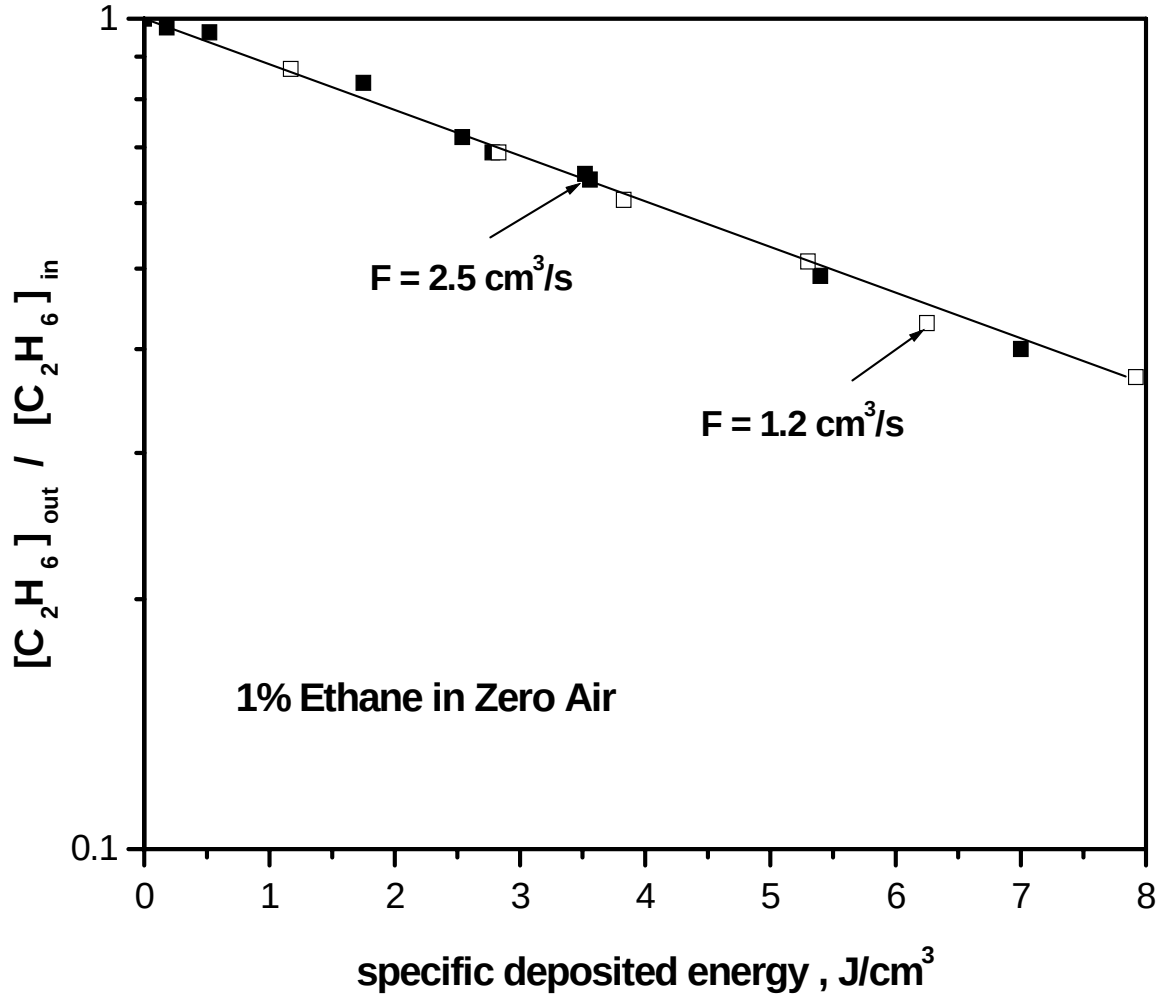
1
0.1
0
1
2
3
4
5
6
7
8
[C2H6]out / [C2H6]in
specific deposited energy , J/cm3
F = 2.5 cm3/s
F = 1.2 cm3/s
1% Ethane in Zero Air

Figure 4

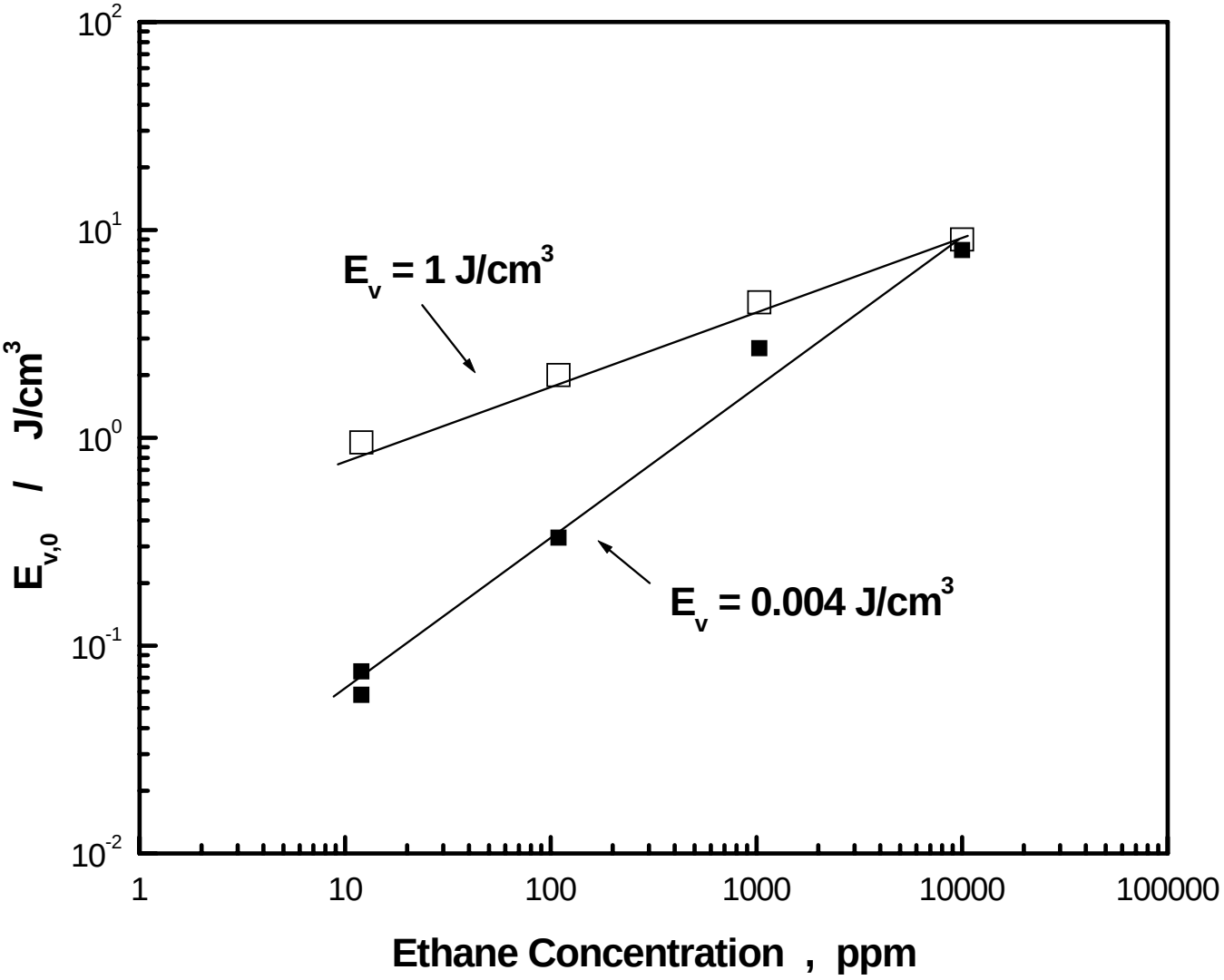
10^2
10^1
10^0
10^{-1}
10^{-2}
$E_{v,0}$ / J/cm^3
E_v = 1 J/cm^3
E_v = 0.004 J/cm^3
1
10
100
1000
10000
100000
Ethane Concentration , ppm

Figure 5

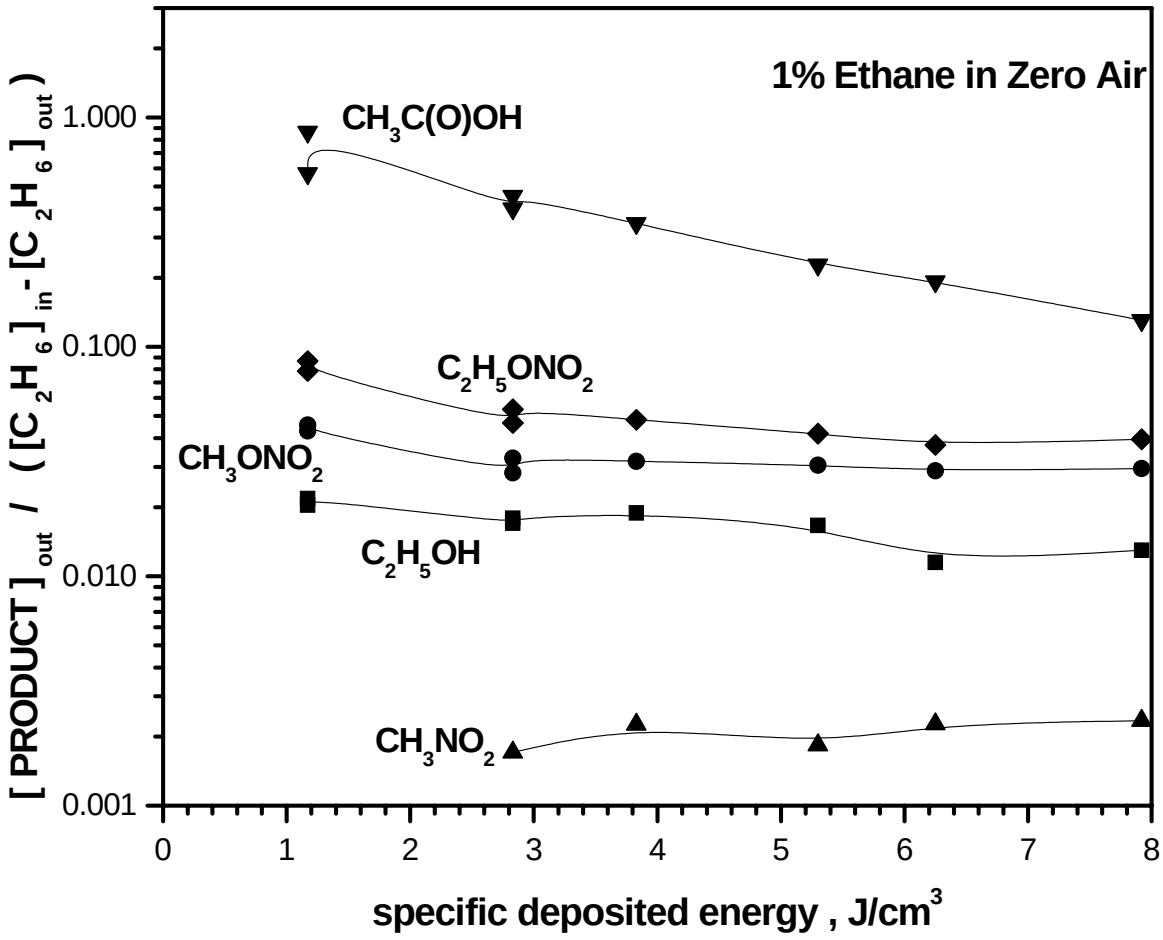
1% Ethane in Zero Air
CH3C(O)OH
C2H5ONO2
CH3ONO2
C2H5OH
CH3NO2
[PRODUCT]out / ([C2H6]in - [C2H6]out)
1.000
0.100
0.010
0.001
0
1
2
3
4
5
6
7
8
specific deposited energy , J/cm3

Figure 6

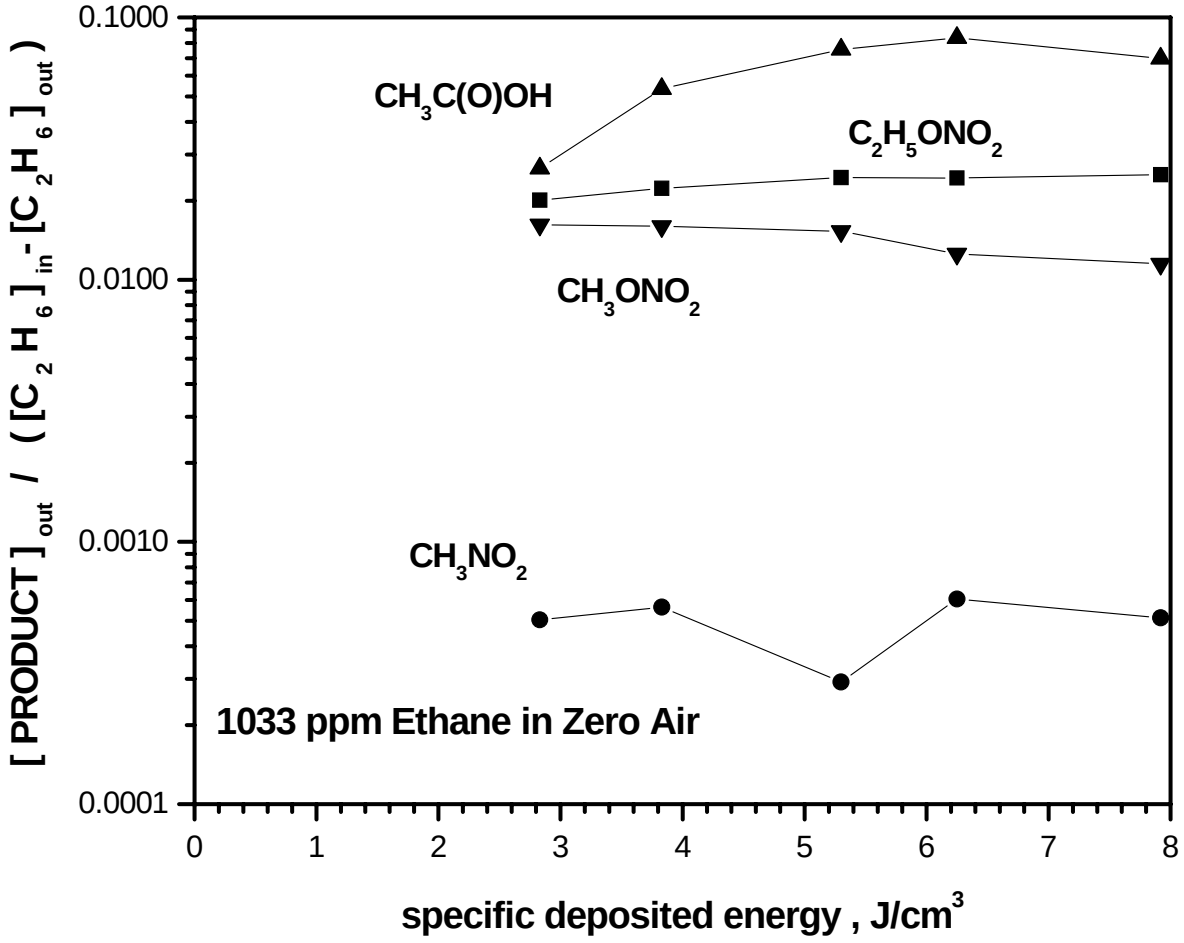
0.1000
0.0100
0.0010
0.0001
0
1
2
3
4
5
6
7
8
[PRODUCT]out / ([C2H6]in - [C2H6]out)
specific deposited energy , J/cm3
CH3C(O)OH
C2H5ONO2
CH3ONO2
CH3NO2
1033 ppm Ethane in Zero Air

Figure 7

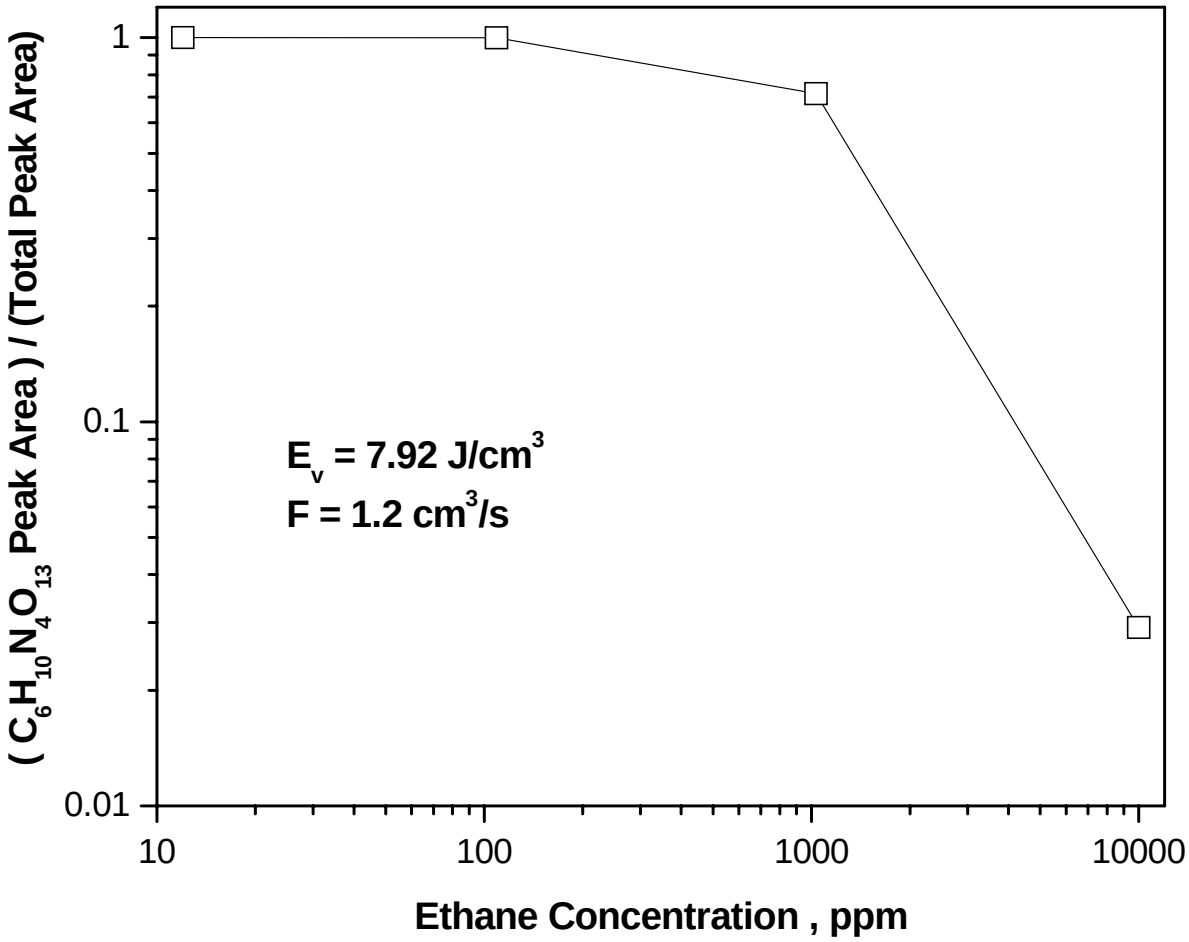
1
0.1
0.01
10
100
1000
10000
(C6H10N4O13 Peak Area) / (Total Peak Area)
Ethane Concentration , ppm
Ev = 7.92 J/cm3
F = 1.2 cm3/s

Figure 8